Modeling Earth Systems and Environment
https://doi.org/10.1007/s40808-018-0420-6

ORIGINAL ARTICLE

Hurricane Matthew (2016) and its impact under global warming scenarios

Mansur Ali Jisan[1] · Shaowu Bao[1] · Leonard J. Pietrafesa[1] · Dongliang Shen[2] · Paul T. Gayes[1] · Jason Hallstrom[3]

Received: 9 November 2017 / Accepted: 6 January 2018

Abstract

A coupled atmosphere–ocean model was used to study the impact of future ocean warming, both at and below the water surface, on hurricane track and intensity and the associated coastal storm surge and inundation. A strong Saffir–Simpson Category-5 hurricane, Hurricane Matthew made landfall on the South Carolina (SC) coast of the United States (US) in September 2016 and was used as our study case. Future ocean warming was calculated based on the Inter-Governmental Panel on Climate Change (IPCC) RCP 2.6 and RCP 8.5 scenarios. Validated setup of the model was used to simulate the changes in track, intensity, storm surge, and inundation of Hurricane Matthew under future climate ocean warming scenarios. Results showed that the future ocean warming could make the hurricanes stronger in intensity, which, in turn, will greatly increase subsequent coastal storm surge and inundation. For example, under the RCP 8.5 scenario, Matthew's maximum wind speed would increase by 18 knots (12.97%), its minimum sea-level pressure would deepen by 26 hPa (2.78%), and the coastal area inundated would increase by 70.20% from that of the present day. Moreover, the increases in coastal surge and inundation could likely lead to a downstream blocking of upstream water systems, thereby exacerbating upstream lateral flooding as the rivers go into storage modes; but that potential is beyond the scope of this study.

Keywords Hurricane · Ocean warming · Storm surge · Climate change · Inundation

Introduction

Tropical cyclones (TCs) are one of nature's most devastating natural hazards that kill many people worldwide and incur huge economic losses every year (Emanuel 2003; Das et al. 2016). Coastal storm surge and the subsequent inundation generated by TCs affect around a billion people living in coastal areas. Global warming has the potential to increase both storm surge and inundation both due to the coupled effects of storm intensification and sea-level rise (SLR). A better understanding of how global warming will affect TCs, i.e., track, intensity, landfall locations, and storm surge and inundation, is necessary in the context of projected global warming scenarios. In addition, any climate change adaptation strategy demands proper analyses of how the future change in climate would affect human welfare in sectors such as ecosystems, agriculture, hydrology, health, energy, and industry.

In recent years, several studies have focused on the impact of climate change on TC frequency and intensity (Gualdi et al. 2008; Knutson et al. 2010; Zhao and Held 2010). While it is possible to simulate tropical cyclones in global models to analyze their statistics under different climate scenarios, it is difficult to generate TC events with realistic intensity, an important factor for society (Zhao et al. 2009), due to the low resolution of those global climate models. To reproduce climate change at regional scales, Kimura and Kitoh (2007) and Sato et al. (2007) introduced a dynamical downscaling method, which uses both present re-analysis data and the monthly mean value difference between the state of the present climate and that of the projected future, for creating model forcing data. Emanuel (1987) first projected hurricane intensity changes in an environment of higher greenhouse gas concentrations. Knutson et al. (2010) summarized the literature regarding the relationship between hurricanes and monthly mean sea surface temperature (SST) and suggests

✉ Mansur Ali Jisan
mjisan@g.coastal.edu

[1] Department of Coastal and Marine Systems Science, Coastal Carolina University, Conway, SC 29526, USA

[2] Shanghai Ocean University, Shanghai, China

[3] Florida Atlantic University, Boca Raton, FL 33431, USA

Published online: 17 January 2018

that by the end of the 21st century, the intensity of future hurricanes could increase by 2–11%.

The above-referenced studies employed relationships between SST and the intensity changes of hurricanes. Several studies show that the sub-surface sea temperature (SSST) is also important in the TC intensification process (Emanuel and Živković-Rothman 1999; Bender and Ginis 2000; Shay et al. 2000; Lloyd and Vecchi 2011; Lin et al. 2014; Price 1981). However, a few studies considered SSST in a global warming scenario (Knutson et al. 2010, 2013). During TC genesis and development, energy is supplied from the sea surface to the TC through air-sea sensible and latent heat flux. TC wind stress mixes cooler sub-surface ocean water with the surface water which in turn reduces the SST, also known as the TC-induced ocean cooling effect (OCE). OCE is a function of ocean vertical temperature profile, size, and intensity of TC and its phase speed (Emanuel and Živković-Rothman 1999; Bender and Ginis 2000; Shay et al. 2000; Lloyd and Vecchi 2011; Lin et al. 2014, 2009; Price 1981; Cione and Uhlhorn 2003). A stronger OCE leads to a less supply of energy into the TC and thus suppresses the intensification process.

To represent the OCE process appropriately, a coupled atmosphere–ocean modeling approach is required. The standalone atmospheric simulations cannot address the effect of OCE, since the sub-surface ocean variations are artificially excluded. Some studied the impact of ocean warming, both at the surface and sub-surface, on TC intensities. Using the Coupled Model Inter-comparison Project Phase 2 (CMIP2) to provide the initial conditions, Knutson et al. (2001) found a minor impact of sub-surface temperature change on TC intensity but recommended a reinvestigation when improved ocean condition estimates become available. Emanuel (2013) made coupled model projections, but he used fixed sub-surface conditions, and therefore, the impact associated with sub-surface temperature changes was not assessed. To overcome these above-mentioned limitations, a coupled ocean–atmosphere model was developed and utilized in this research.

The oceanic component included the projections of future ocean warming at the surface and the sub-surface downward to the depth of 1000 m, based on IPCC's fifth assessment report (AR5, Stocker 2014), which states that the ocean will continue warming during the 21st century and the increased heat will penetrate from the surface into the deeper water column and affect ocean circulations at those deeper depths. The IPCC report also predicts that in the future, TCs could increase in intensity, resulting in stronger peak wind speeds and heavier rainfall (Rahaman et al. 2016). In this study, we utilized the projections from IPCC's RCP 2.6 and RCP 8.5 scenarios as the oceanic initial conditions and used the coupled atmosphere–ocean model to simulate Hurricane Matthew. The objective is to assess how a TC similar to Hurricane Matthew, and its associated storm surge and inundation, would behave under future climate conditions with warmer ocean water.

The structure of the paper is as follows: the development and architecture of a coupled atmosphere–ocean model and methods used to prognosticate future ocean water warming are described in Sect. "Methodology". In Sect. "Results", we utilize observations to validate Hurricane Matthew's track, intensity and associated storm surge under the present-day conditions. In addition to that, sensitivity analysis due to the coupling of ocean model with the atmosphere is analyzed. This section also includes the results based on future projections. Using the validated setup of the models, we make future projections of track, intensity, storm surge, and inundation. Discussion on uncertainties associated with the results and oceanic response under future RCP scenarios are presented in Sect. "Discussion". Concluding remarks are presented in Sect. "Conclusion".

Methodology

Description of numerical model

The interactively coupled atmosphere–ocean model

An interactively coupled atmosphere–ocean model system was used to simulate the track and intensity of Hurricane Matthew under the present-day and future climate scenarios. This system was previously used in several studies (Jisan et al. 2016; Bao et al. 2017) to investigate the oceanic response to the passages of storms in differing locales.

This coupled modeling system features an air-sea coupler that connects the atmospheric and the oceanic modules. The coupler and the constituent modules are all coupled using the Earth System Modeling Framework (ESMF, Hill et al. 2004). The Weather Research and Forecast (WRF; version 3.7.1) model with the Advanced Research WRF (ARW) dynamical core (Skamarock et al. 2005) was used as the atmospheric module. WRF is non-hydrostatic, a quasi-compressible model with multiple physics parameterization schemes as well as the capability of storm following and moving nest for hurricane modeling. For the oceanic component, Regional Ocean Modeling System (ROMS) version 3.3 was used. ROMS is a free surface, terrain-following numerical model that is capable of solving the three-dimensional Reynolds-averaged Navier–Stokes equations using hydrostatic and Boussinesq approximations (Temam 1984). Multiple turbulence models, advection schemes, lateral boundary conditions, and surface and bottom boundary layer schemes are implemented in ROMS.

ESMF-based coupled geophysical model systems follow a standardized architecture, where the constituent modules,

such as WRF and ROMS, are assembled by the ESMF superstructure (Balaji and Numrich 2005). The ESMF superstructure's classes, including the import or export state, gridded-component, and coupler-component, provide methods for data exchange between constituent geophysical modules.

The gridded components encapsulate the details in the constituent modules, so that they can perform the following three standardized functions: initialization (*ESMF_GridComInitialize)*, integration (*ESMF_GridCompRun)*, and finalization (*ESMF_GridCompFinalize)*. The import or export state classes contains the information that will be exchanged between constituent modules. The import state contains the input data required for the component to run, and the export state contains the data that the component produces and sends to other components as their import state. When a gridded-component integrates, it communicates with other gridded components through a standardized interface: it reads in an import state class and writes an export state class. The coupler-component remaps the import and export state classes onto different model grids when the constituent modules are on different domains.

Specifically, Fig. 1 shows the flowchart of coupling WRF and ROMS, and what variables are exchanged between them. The coupler-component first creates two ESMF-gridded components for the two constituent modules, one representing WRF, the other ROMS. As mentioned earlier, the WRF- and ROMS-gridded components are encapsulated into the three top-level compartments, performing the model's "initialization", "integration", and "finalization" functions. The coupler-component also creates the import and export state classes for each gridded component. Next, the WRF and ROMS execute their "initialization" methods respectively to assign the initial values to the atmosphere and ocean state variables.

After the WRF- and ROMS-gridded components are initialized, they start forward integration. After each timestep, the momentum and thermal exchange coefficients are calculated based on the stability functions of the similarity theory (Paulson 1970; Dyer and Hicks 1970; Webb 1970). Using these coefficients, the momentum and heat fluxes through the atmosphere–ocean interface are calculated in WRF, using the Noah LSM model (Chen and Dudhia 2001). The underlying sea surface temperature (SST) and current (SSC) is used in the calculations of the fluxes. The fluxes calculated in WRF are added to its *export* state, which is later received by the ROMS as its *import* state. In ROMS, the fluxes received from WRF are then used as its surface wind and heat forcing for its integration. During ROMS integration time step, it writes SST and SSC into its *export* state, which is later received by WRF as its *import* state and read into the WRF component. Thus, the WRF and the ROMS exchange surface wind and SST fields at each time step. The SST and SSC are then used by WRF in its calculation of surface

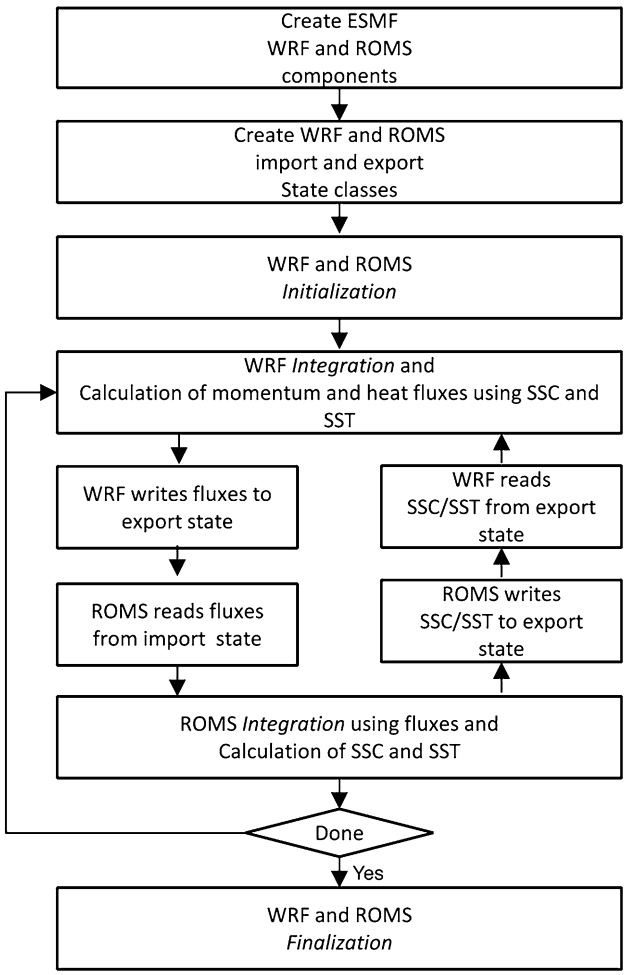

Fig. 1 Diagram of the WRF–ROMS coupling using the ESMF-based coupler

fluxes. When the integration time limit is reached, the time iteration stops and the coupler proceeds to the "Finalize" stage, which starts the "wrf_finalize" and "ROMS_finalize" routines to finish the entire simulation.

Delft3D-flow

Delft3D-FLOW (Delft WL | Delft Hydraulics, The Netherlands) was used to simulate storm surge and inundation. The model is a hydrodynamic and transport simulation program that calculates non-steady flow and transport phenomena resulting from astronomical tidal and meteorological forcing. It solves the unsteady shallow water equations, including the horizontal equations of motion, the continuity equation, and the transport equations for conservative constituents. The equations are formulated in orthogonal curvilinear coordinates or in spherical coordinates on the globe. Delft3D—FLOW can be applied for modeling tidal waves, storm surges, tsunamis, harbor oscillations (seiches),

and the transport of pollutants in vertically well-mixed flow regimes. The wind speed and sea-level pressure generated from the coupled atmosphere–ocean model were used as input in Delft3D to simulate the storm surge and inundation.

Domain and model configuration

The WRF model has a fixed outer domain with a 6-km grid-spacing (430 × 512 grid points) and a vortex following moving nest domain with a 2-km grid-spacing (271 × 271 grid points) (Fig. 2). The WRF domains have 36 vertical levels with a terrain-following sigma coordinates. The inner domain was updated every 15 min.

In the coupled atmosphere–ocean model, the WRF component employs the WSM3 microphysics scheme (Hong and Lancaster 2004). For long-wave and short-wave radiation calculations, the Rapid Radiative Transfer Model (RRTM, Mlawer et al. 1997) and Dudhia schemes (Dudhia 1989) were used. The YSU Planetary Boundary Layer (Noh et al. 2003) scheme was used as the thermal diffusion scheme to represent surface physics. The initial and boundary conditions for the WRF model simulations were derived from the 1 × 1-degree NCEP global Final Analysis (FNL) which was processed using WRF post-processing (WPS).

The ROMS model domain is the same as the WRF's outer domain. ROMS employed 36 stretched terrain-following vertical levels. The initial and boundary conditions were obtained from the 1/12°, global Hybrid Coordinate Ocean Model with Naval Research Lab Coupled Ocean Data Assimilation (HYCOM/NCODA) solutions. In the ROMS simulation, a 24 s time step was used.

For the storm surge and inundation component Delft3D-FLOW, a separate grid and bathymetry were constructed over the coast of South Carolina (SC) and part of North Carolina (NC), up to Jacksonville (Fig. 3). National Geophysical Data Center's Coastal Relief Model (Divins and Metzger 2008) was used as the topography and bathymetry source. The grid cell resolution of the Delft3D grid varies from 156 to 1200 m with higher resolution applied over the land to simulate the storm surge and inundation accurately. To simulate storm surge and inundation, Delft3D's wind speed and pressure input were extracted from the coupled atmosphere–ocean model. Other physical parameters considered in the storm surge simulation were Manning's

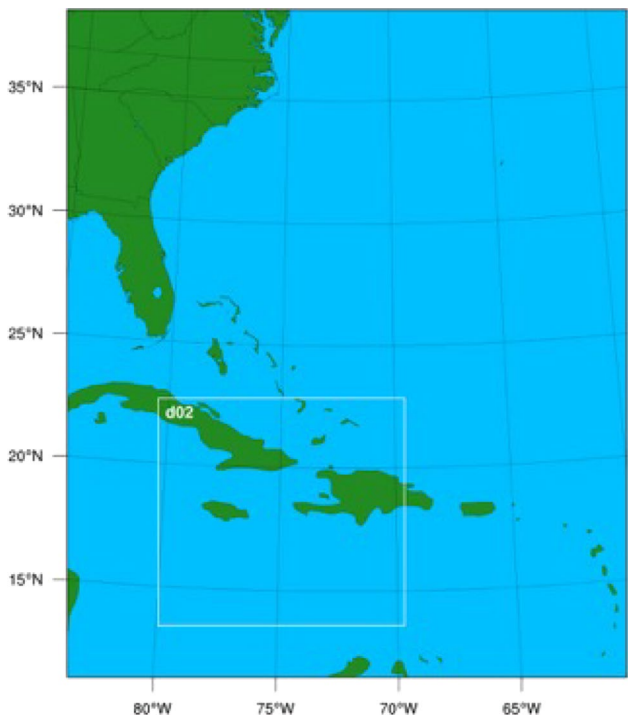

Fig. 2 Extent of the model domain used for the WRF and ROMS simulation. The white square box (d02) inside the outer domain is the initial location of the vortex, subsequently following the moving nest, which was updated at every 15 min following the movement of the storm throughout the simulation period

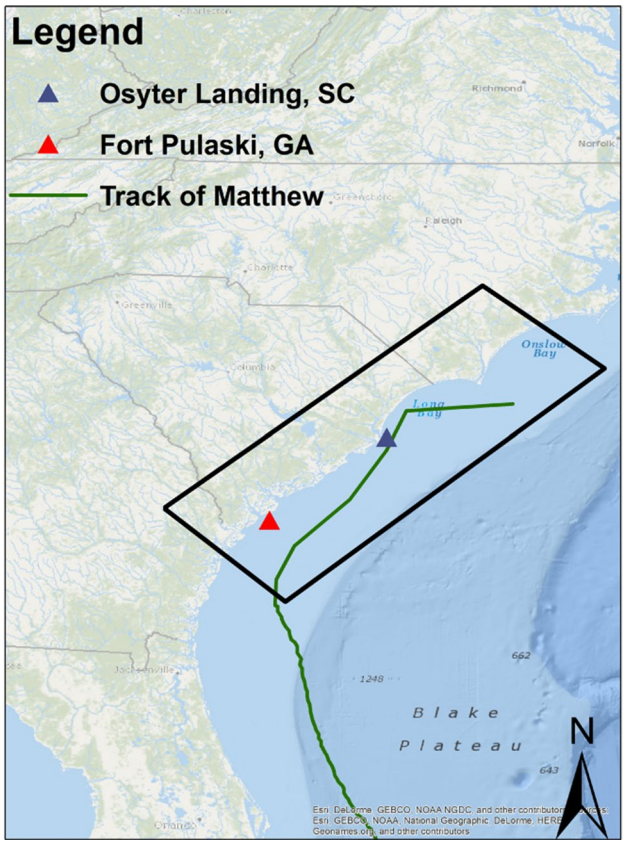

Fig. 3 Study area for storm surge and inundation. The black colored outline is representing the extent of a Delft3D grid. Red and blue triangles are representing the tide station used for validating the storm surge level. The green line is representing the observed track of Hurricane Matthew

roughness coefficient, gravity, horizontal eddy viscosity and diffusivity, and the density of water and air.

Future ocean warming scenarios and experimental design

According to IPCC's 5th assessment report, increases of 0.6 °C (RCP 2.6) up to 2 °C (RCP 8.5) were projected for the top 100-m depth of the ocean. From that depth, down to the 1000-m depth, the projected change is 0.3 °C (RCP 2.6) to 0.6 °C (RCP 8.5). To represent the future ocean warming scenarios, the present-day oceanic initial temperature was increased both at the surface and the sub-surface layers based on the projections from the RCP 2.6 and RCP 8.5 scenarios (Table 1). For the atmospheric components, the initial conditions were kept the same as the present-day conditions, but they were influenced by the change in ocean heat content, since both components are interactively coupled with ESMF.

Table 1 Ocean temperature conditions for simulating the future scenario of Hurricane Matthew under present-day, RCP 2.6, and RCP 8.5 scenarios

Climate scenarios	Temperature increase (°C)	
	0–100 m	101–1000 m
Present-day	0.0	0.0
RCP 2.6	0.6	0.3
RCP 8.5	2	0.6

To generate the future storm surge and inundation scenarios, the simulated track and intensity of Hurricane Matthew under the RCP 2.6 and RCP 8.5 scenarios were used as input to Delft3D FLOW. The objective of this experiment is to evaluate how much additional area would get inundated due to the changed intensity of the storm under future ocean warming scenarios.

Results

Validation of the model result

Track and intensity

The simulated track of Hurricane Matthew agreed reasonably well with the actual track determined after the fact by the NOAA National Hurricane Center (NHC; Stewart 2017) (Fig. 4a). Track errors were calculated at 6-h intervals (Fig. 4b), which showed that at the time of landfall, the track error was much less (~ 8 km) than at the other times. This accurately modeled landfall location was important for storm surge simulation.

From Fig. 5, we can see that the model simulated the peak intensity well enough, except that the initial strength was weaker than the observed, which was due to the weak

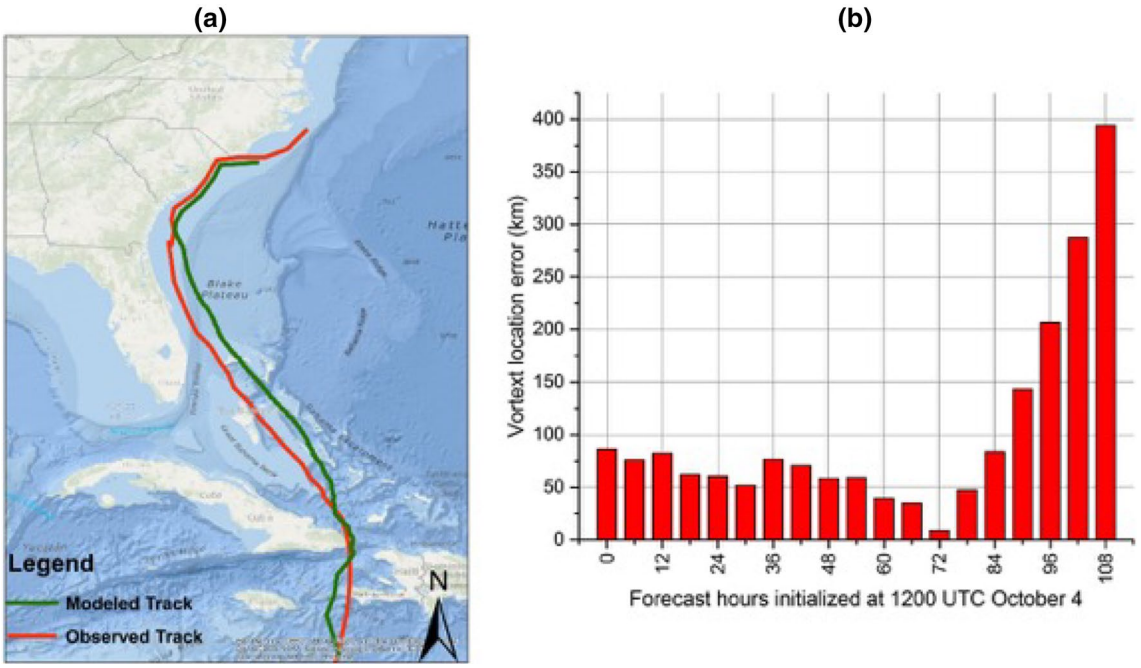

Fig. 4 **a** Comparison of the simulated track of Hurricane Matthew with respect to that observed (source is NHC). **b** Vortex location error (kilometers) calculated at 6-h intervals with respect to the NHCs observed track

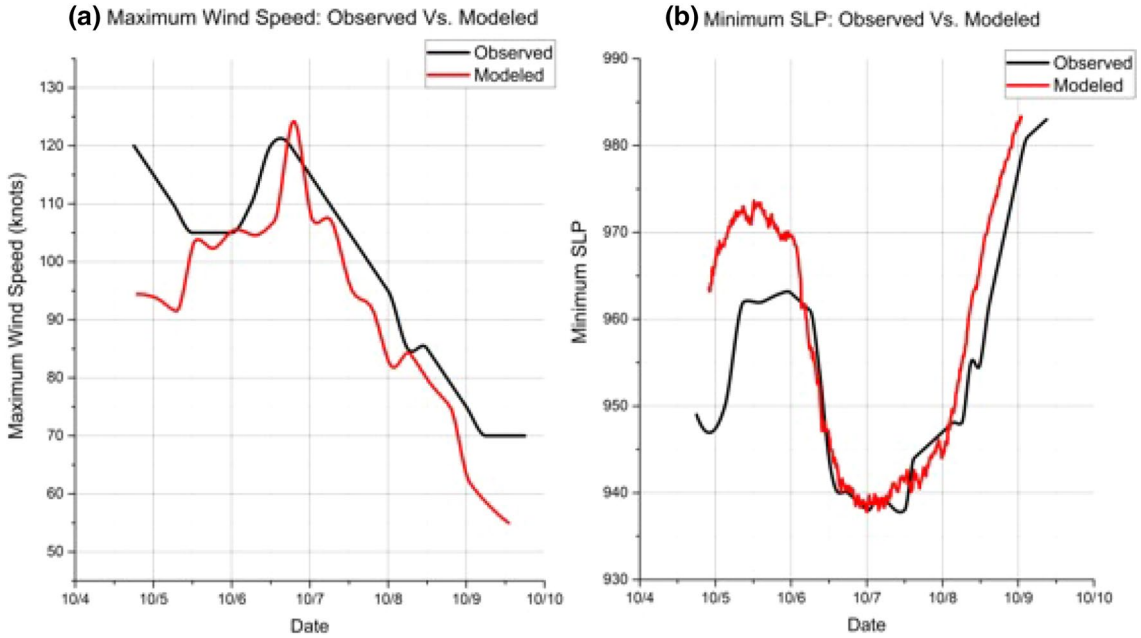

Fig. 5 Comparisons of **a** model-simulated wind speed and minimum sea-level pressure of Hurricane Matthew versus observations. **a** Comparisons of maximum wind speeds (knots). **b** Comparisons for minimum sea-level pressure (hPa)

vortex in the FNL input data and the lack of vortex initialization techniques. During the landfall on October 8, the model simulated the wind speed accurately, which is important for simulating the storm surge and inundation accurately. The simulated MSLP is consistent with the peak wind speed. The model simulated the MSLP appropriately on October 7, but following landfall on October 8, it began to show differences from the observed MSLP; likely caused by the difference between the simulated and observed tracks. Since this paper is focused on the impact of ocean warming on storm surge and inundation, the track and intensity at the landfall time were simulated well enough to be used in the subsequent experiments.

Storm surge

The simulated storm surge height was validated using the hourly tide data from NOAA's National Oceanographic Services (NOS) at Fort Pulaski in Georgia (GA) and Oyster Landing in SC, both sites along the path of Hurricane Matthew (Fig. 6). The model accurately simulated the peak water level (2.25 m) for Fort Pulaski. For Oyster Landing, it overestimated the peak water level by 0.53 m (3.12 m). A finer resolution of bathymetry could help to reduce the errors. Nevertheless, the calculated Root Mean Squares for Fort Pulaski and Oyster Landing are 0.08 and 0.13 m respectively, both deemed reasonably representative for the existing setup of the model to be used for simulating future changes in storm surge and inundation.

Sensitivity analysis due to atmosphere–ocean coupling

As we discussed in the *Introduction* concerning the inability of standalone atmospheric models in simulating the future hurricane intensity change properly, we compared the intensities of Hurricane Matthew generated using the standalone WRF model and the coupled WRF-ROMS model under a present-day scenario. It is to be noted that in the standalone WRF simulation, the SST remains fixed throughout the simulation period. As a result, the dynamic change of SST due to the movement of the storm does not get reflected properly.

Results from the comparison between the standalone WRF model and the coupled WRF-ROMS model were presented in Fig. 7. The figure shows that the standalone WRF model overestimated the peak wind speed by 16.42 knots (13.2%) and MSLP deepening by 4.96 hPa (0.53%), compared with the coupled atmosphere–ocean model simulation. This overestimated intensity in the standalone WRF simulation was caused by the missing OCE, which was represented in the coupled simulation by introducing a separate ocean component in it. The better representation of the OCE thus allows us to investigate the underlying reasons behind the change in intensity of the storms. Hence, the system was applied to make future projections.

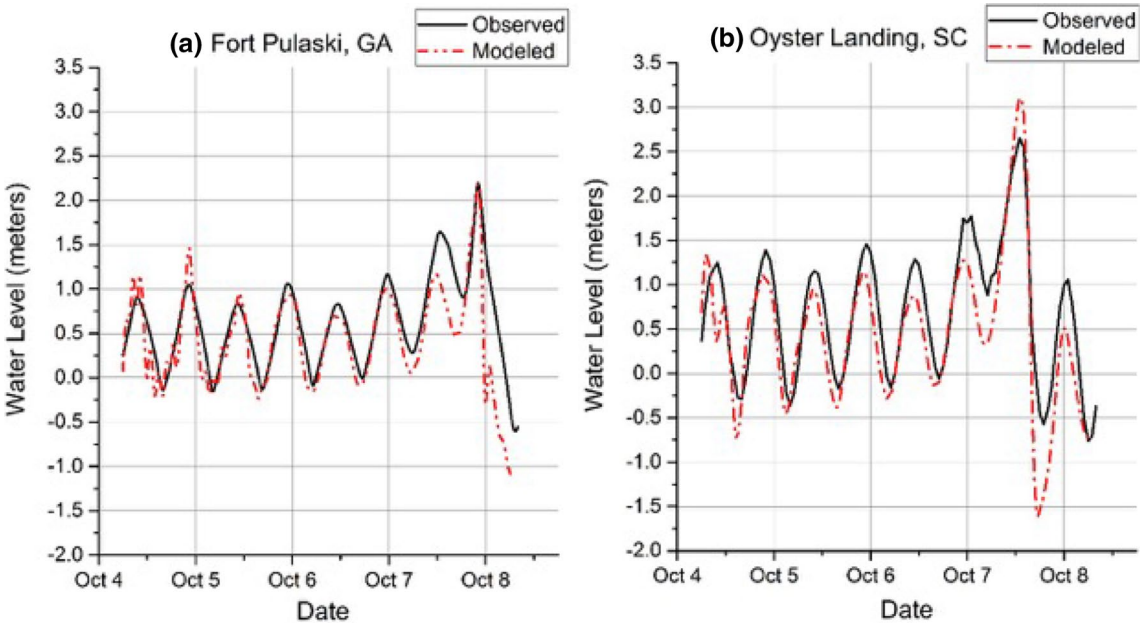

Fig. 6 Comparisons for model simulated storm surge of Hurricane Matthew with the observed water level from National Oceanographic Services. **a** Fort Pulaski GA station. **b** Oyster Landing SC station

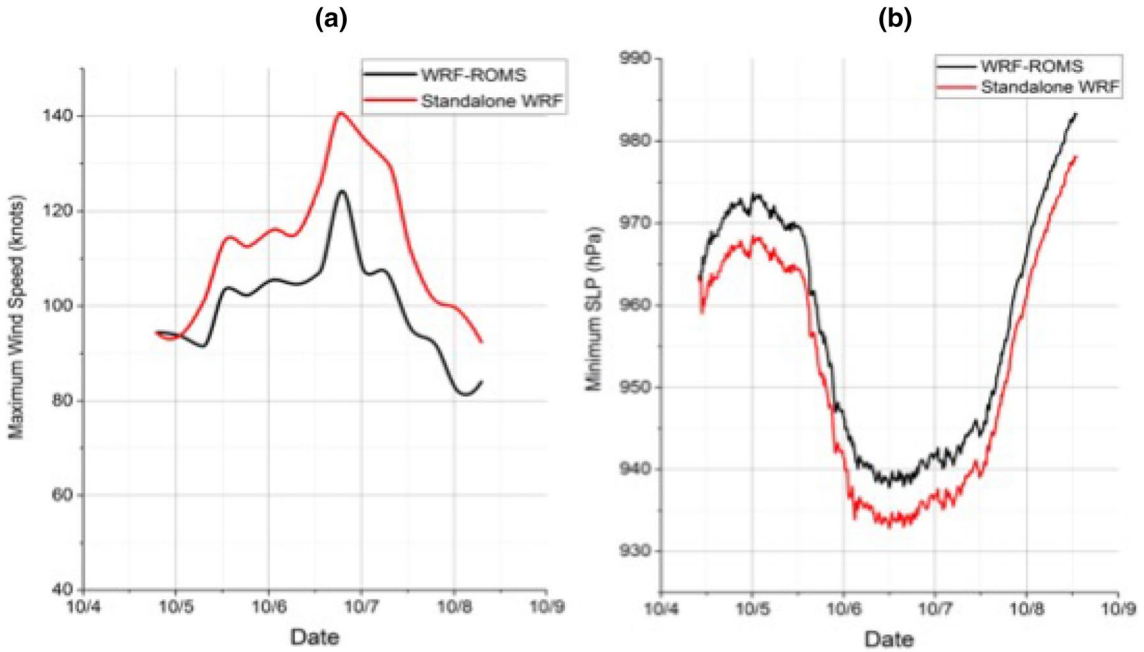

Fig. 7 Simulations of peak winds and lowest central pressures of Hurricane Matthew for the cases of WRF per se and for the coupled WRF-ROMS models: **a** peak wind speeds and **b** minimum MSLP

Future changes of hurricane matthew under the global warming scenario

Track and intensity

Figure 8 shows the tracks of Hurricane Matthew under the RCP 2.6 and RCP 8.5 ocean warming scenarios and the present-day track. The track generated under RCP 2.6 (where the temperature in the upper 100 m was increased by 0.6 °C and the sub-surface water column temperature below 100 m was increased by 0.3 °C) shows only a slight difference with the present-day, and the landfall location was close to the

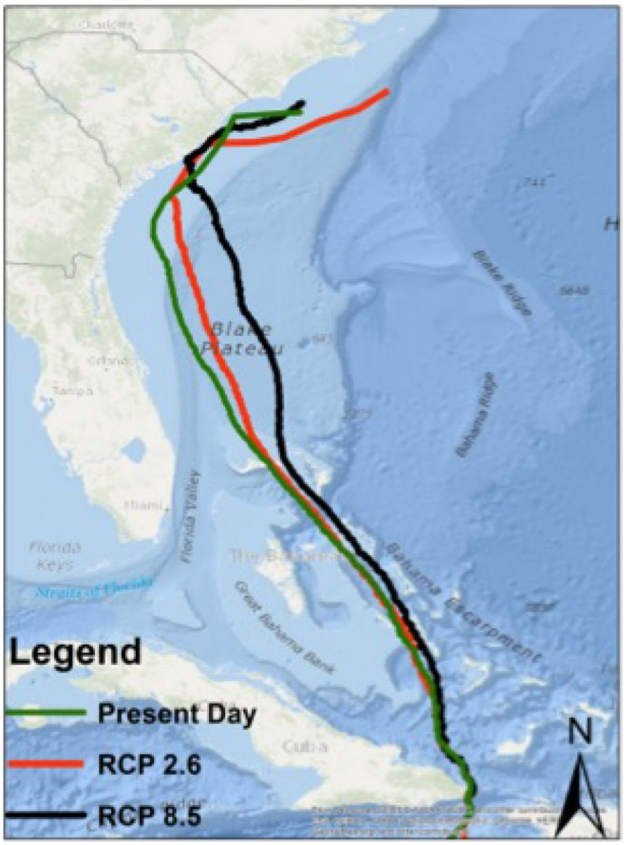

Fig. 8 Simulated tracks of Hurricane Matthew for the cases of present-day (green); under the RCP 2.6 scenario (red); and under the RCP 8.5 scenario (black)

actual landfall location, McClellanville SC. Alternatively, the track generated under the RCP 8.5 scenario (where the temperature of the upper 100 m was increased by 2 °C and the water temperature below 100 m was increased by 0.6 °C) follows the route of the present-day track until the TC reached the Florida Valley. After crossing Florida Valley, the TC took a slight North-Eastward turn and made landfall at the Charleston Harbor of South Carolina. These changes could be influenced by the warmer oceanic surface water and also due to the relatively higher temperatures in the cold-water wake, which was interacting with the atmosphere, due to the coupling effect.

As shown in Fig. 9a, under RCP 8.5, the maximum wind speed of Matthew would increase due to the effects of ocean warming. The peak wind speed would be 18 knots stronger (12.97%) than the present-day. Under RCP 2.6, the change in peak intensity was 6 knots stronger (5.41%) than the present-day, as shown in Fig. 9a. In Fig. 9b, we see that the MSLP reached a minimum value of 936 hPa (0.43% lower than present) and 912 hPa (2.78% lower than present-day) for RCP 2.6 and RCP 8.5 scenarios.

Storm surge and inundation under future climate scenarios

Future storm surge levels

Figure 10 shows the peak storm surge levels of the Oyster Landing SC and Fort Pulaski GA stations simulated by the Delft-3D model using the simulated track and intensity of Hurricane Matthew under the present-day, RCP 2.6, and RCP 8.5 scenarios. Results show that storm surge

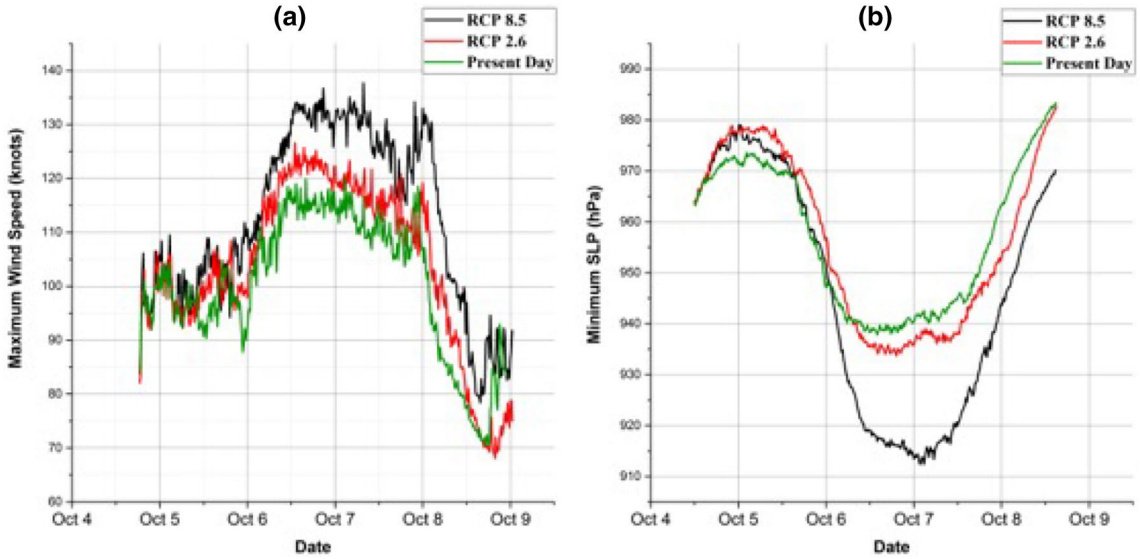

Fig. 9 Simulated Hurricane Matthew peak wind speed (knots) (**a**) and MSLP (hPa) (**b**) under the present-day and future RCP scenarios. Blue lines are for the present-day, red for RCP 2.6, and black for RCP 8.5

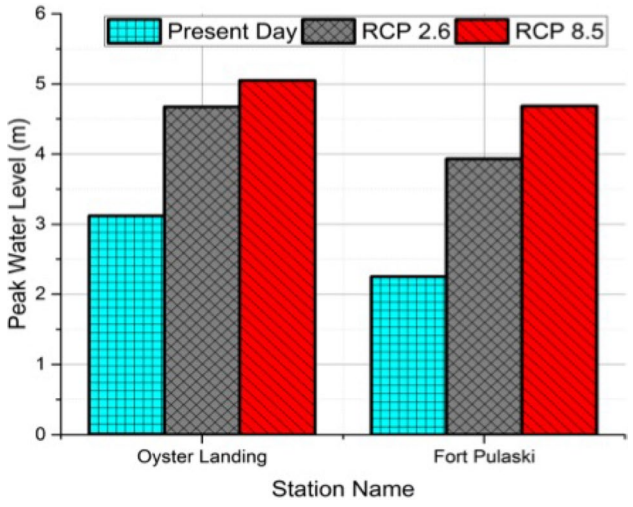

Fig. 10 Comparisons of peak water levels at Oyster Landing SC and Fort Pulaski GA stations based on the simulated track and intensity of Hurricane Matthew at cases of the present-day and under future RCP scenarios

levels would increase under the influence of the increased intensity under the RCP scenarios. Peak water level for the Oyster Landing station, which was simulated 3.12 m in the present-day climate, would reach 4.67 m (49.6% more than present) and 5.05 m (61.8% more than present) for the RCP 2.6 and 8.5 scenarios respectively. Similarly, for the Fort Pulaski station, peak water level would increase by 74.6% (3.93 m) and 108% (4.68 m) for the RCP 2.6 and 8.5 scenarios, respectively.

Future inundation areas

As shown in the previous section, due to the increased intensity of Hurricane Matthew under RCP warming scenarios, the peak storm surge level will increase significantly, which will also lead to increased inundation areas; and likely increased upstream, inland lateral flooding. In this section, we evaluate how the changed intensity will also influence the coastal zone inundated areas.

Due to the increased intensity, the inundated area under the RCP ocean warming scenarios would also become higher than that under the present-day condition. Figure 11 shows the comparisons of the inundated area under present-day and RCP scenarios. The model simulated inundated areas are 95.60, 125.16 km^2 (30.92% more than present-day), and 162.72 km^2 (70.20% more than present-day) for the present-day, RCP 2.6 and RCP 8.5 scenarios, respectively. In the RCP 8.5 scenario, the inundated area extended towards the northeast, because the simulated Hurricane Matthew made landfall slightly towards that direction (Fig. 11c) compared with the simulated tracks under the present-day and RCP 2.6 scenarios (Fig. 11a, b).

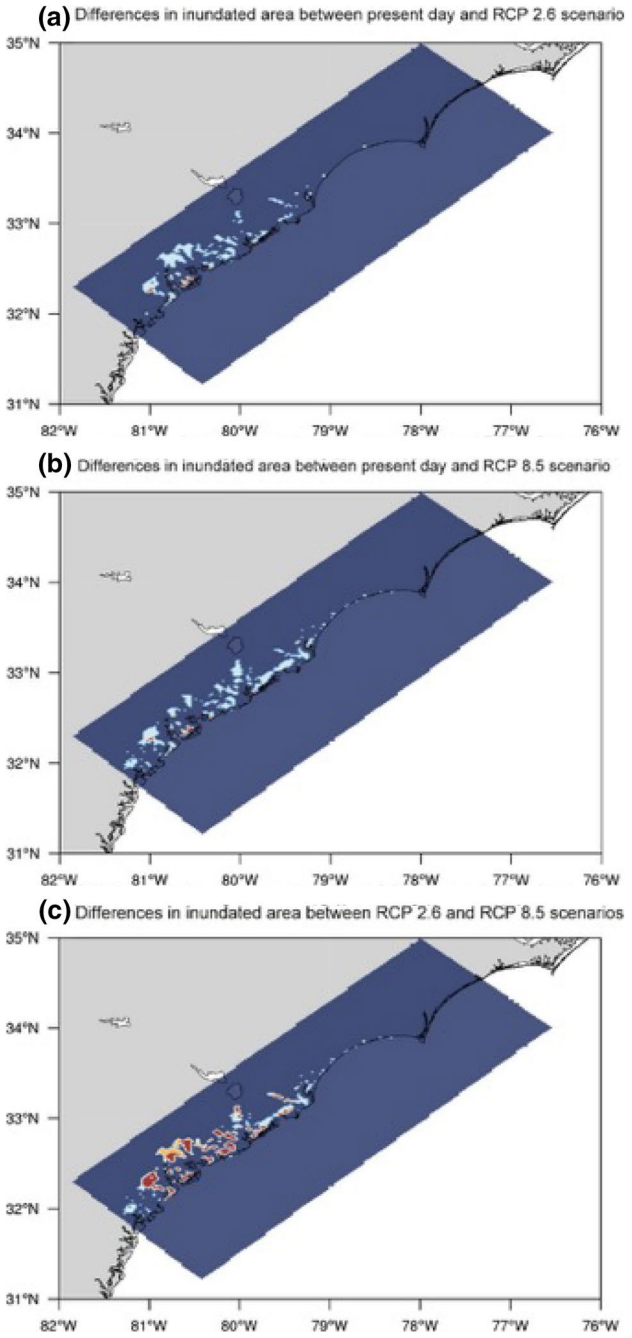

Fig. 11 Simulated inundated areas under **a** the present-day and the RCP 2.6 scenarios; **b** the present-day and RCP 8.5 scenarios; and **c** RCP 2.6 and RCP 8.5 scenarios. Dark blue-colored areas are the non-flooded areas. White areas are inundated under RCP scenarios but not in the present-day. Red shows the areas inundated under both the RCP and present-day scenarios. The yellow areas are inundated using the present-day case but under the two RCP scenarios

Discussion

We showed that under future ocean warming scenarios, the intensity and the associated storm surge and inundation

for a storm similar to Hurricane Matthew would become higher than the present-day.

To understand the impact of ocean warming on simulated hurricane intensity, we analyzed the areas of the cold-water wake upon the ocean surface. Figure 12 shows the simulated change in SST caused by Hurricane Matthew under the present-day and RCP 2.6 and RCP 8.5 scenarios. A decreasing trend in the cold-water wake can be noticed for the future RCP scenarios comparing it with the actual present-day scenario. The red-colored area, which was cold water with a cooling of ≥ 2.0 °C, was smaller in the RCP 2.6 scenario than in the case of present-day conditions (Fig. 12a, b) as well as in the RCP 8.5 scenarios than in the RCP 2.6 scenario (Fig. 12b, c). Since upwelling of cold deep ocean water helps to suppress the Hurricane intensity, this reduction in cold water zone associated with a warming ocean water was the main reason behind the increased simulated intensity of Hurricane Matthew under a warmer ocean condition before it made landfall on the SC coast.

The ocean warming's impact on the OCE process can also be seen from the vertical temperature profile under the present-day and RCP scenarios (Fig. 13). The point is located at 27.62°N and 77.57°W, and it was shown as the black dot in Fig. 12 a–c. From Fig. 13, we can see that for scenarios RCP 2.6 and RCP 8.5, the water that was brought up from the deep ocean, as a result of upwelling, was warmer than the present-day. For example, under the RCP 2.6 scenario, for which we increased the water temperature by 0.6 °C up to the depth of 100 m at the initial time, the upwelled water was 0.25 °C warmer (28.25 °C) than the present-day case (Fig. 13a, b). Similarly, water that was brought up under RCP 8.5 was 28.5 °C, which is 0.5 °C warmer than the present-day (Fig. 13a, c). This increase in temperature associated with hurricane-induced upwelling under the RCP scenarios was responsible for the reduction in the area of

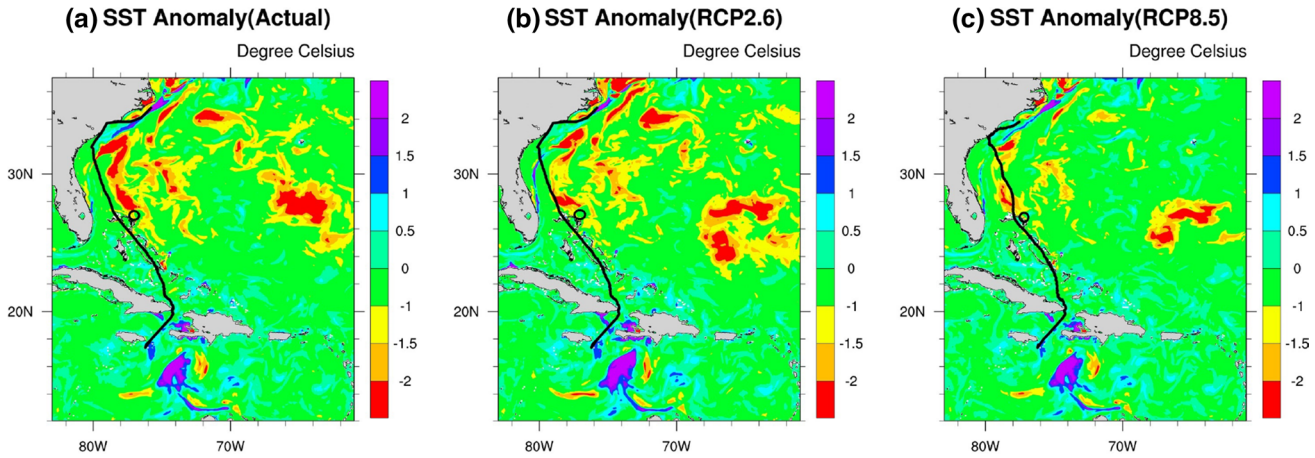

Fig. 12 Change in SST associated with Hurricane Matthew under conditions of **a** present-day conditions; **b** a future RCP 2.6 scenario; and **c** a future RCP 8.5 scenario. The black dot is the point where the vertical temperature profile was analyzed in Fig. 13

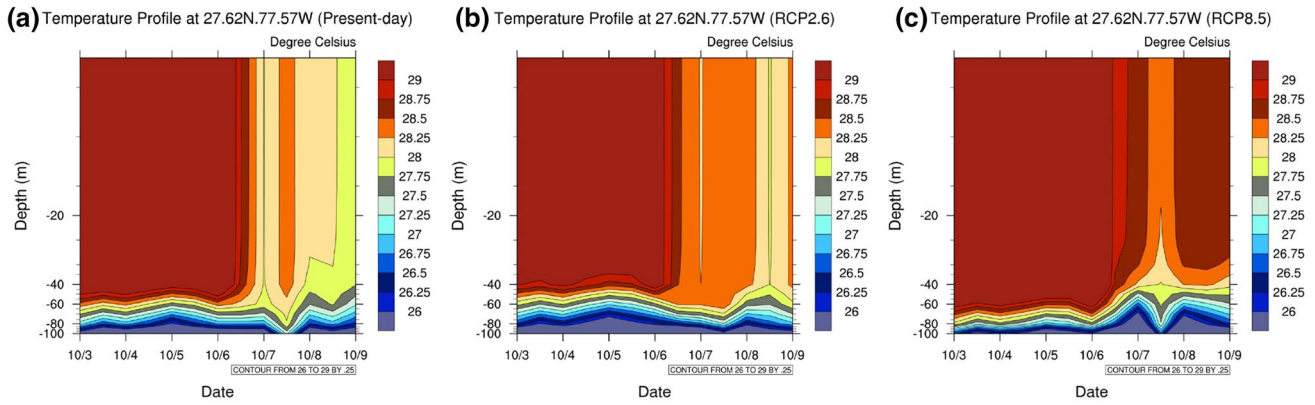

Fig. 13 Time series of the vertical temperature profile at 27.62°N and 77.57°W under **a** present-day conditions; **b** the RCP 2.6 scenario; and **c** the RCP 8.5 scenario

surface cooling shown in Fig. 12, which, in turn, led to the increased intensity of Hurricane Matthew before the hurricane made landfall.

To simulate the future change in track and intensity of Hurricane Matthew, we only considered ocean warming. However, studies suggest that, in addition to SST, air temperature and humidity also can have a significant influence on TC intensification (Knutson and Tuleya 2004). Shen et al. (2000) studied the factors affecting hurricane intensity under the conditions of global warming and conclude that air temperature and SST have contrasting influences on hurricane intensity. In addition, Vecchi et al. (2013), Emanuel et al. (2013), and Wang et al. (2014) find that changes in the vertical profile of air temperature near the tropopause affect TCs.

There are some limitations in this study. For storm surge and inundation under future RCP scenarios, we have only considered the increased intensity of Hurricane Matthew, but we did not include the effect of sea-level rise (SLR). The effect of SLR could make the surge height higher and the inundated areas larger (Williams et al. 2015). For example, under RCP 2.6, the simulated inundated area was 198.16 km^2, but if we would also consider the projected 0.26 m SLR for a mid-21st century under that RCP 2.6, the inundated area would be 406.25 km^2, an increase that would make the inundation greater. In addition, in making future projections of storm surge and inundation, an ensemble of simulations, each with different tracks, intensities, and times, would reduce the uncertainties associated with landfall location, strength, and tide conditions, as shown by Jisan (2017) and Jisan et al. (2017; under review). For instance, the impact of Hurricane Matthew would be less if it had made landfall in low tide or zero tides, and worse during high tides. Since Hurricane Matthew was a Category 5 and made landfall at high tide, this study presented a worst-case scenario. Furthermore, according to the U.S. Forest Service, in the RCP 2.6 scenario, a total of 23 million acres of forest land loss are projected for the Southeast U.S. For heavily forested SC, the loss in forests is predicted to be ~ 11 million acres (Wear and Greis 2012) in and of itself. In addition, Yospin et al. 2015 showed that under future climate change scenarios vegetation will decrease significantly. This potential future land-use change would increase the risk of storm surge threat, since forests work as a buffer against storm surge and inundation (Sakib et al. 2015; Jisan et al. 2017).

Conclusion

A coupled atmosphere–ocean model was developed and applied to simulate the future track and intensity of Hurricane Matthew, and the associated storm surge and inundation, under warmer ocean condition based on the IPCC RCP 2.6 and RCP 8.5 scenarios. The results showed that, with warmer ocean waters, both surface and sub-surface, the peak wind speed would increase within the range of 6–11 knots and the MSLP would deepen within the range of 2–26 hPa. These intensity changes influenced the simulated hurricane-induced storm surge and inundation. Storm surge level would change by 49.60–108% and the inundated area would change by 30.92–70.20%. Thus, TC-induced storm surges and inundation along the SC coast could be higher in the future under different global warming scenarios, particularly for the RCP 8.5 scenario. These results could provide an effective tool for policymakers, emergency managers, and other local government agencies to make proper arrangements regarding disaster preparedness plans.

Acknowledgements The National Science Foundation (NSF) is acknowledged for undergirding this research effort. Coastal Carolina University's (CCU) Cyber Infrastructure Project is used to perform the simulations in this study, which is funded by NSF Major Research Instrument under contract AGS-1624068. Two NSF awards supporting the investigations of the processes of storm-induced coastal surge and inundation and inland flooding are CNS-1541917 and CNS-1713922. The SC State Guard is acknowledged for encouraging that prognostic studies such as this be conducted, so that they may be better prepared for future environmental hazardous events. CCU is acknowledged for providing the facility computational time support for this study.

References

Balaji V, Numrich RW (2005) A uniform memory model for distributed data objects on parallel architectures. In: Use of high-performance computing in meteorology. World Scientific, pp 272–294

Bao S, Li X, Shen D, Yang Z, Pietrafesa LJ, Zheng W (2017) Ocean upwelling along the Yellow Sea coast of China revealed by satellite observations and numerical simulation. IEEE Trans Geosci Remote Sens 55(1):526–536. https://doi.org/10.1109/TGRS.2016.2610761

Bender MA, Ginis I (2000) Real-case simulations of hurricane-ocean interaction using a high-resolution coupled model: Effects on hurricane intensity. Mon Weather Rev 128(4):917–946. https://doi.org/10.1175/1520-0493(2000)128%3C0917:RCSOHO%3E2.0.CO;2

Chen F, Dudhia J (2001) Coupling an advanced land surface–hydrology model with the Penn State–NCAR MM5 modeling system. Part I: Model implementation and sensitivity. Mon Weather Rev 129(4):569–585. https://doi.org/10.1175/1520-0493(2001)129%3C0569:CAALSH%3E2.0.CO;2

Cione JJ, Uhlhorn EW (2003) Sea surface temperature variability in hurricanes: Implications with respect to intensity change. Mon Weather Rev. https://doi.org/10.1175//2562.1

Das Y, Mohanty UC, Jain I (2016) Development of tropical cyclone wind field for simulation of storm surge/sea surface height using numerical ocean model. Model Earth Syst Environ 2(1):13. https://doi.org/10.1007/s40808-015-0067-5

Divins DL, Metzger D (2008) NGDC coastal relief model. National Geophysical Data Center, National Oceanic and Atmospheric Administration, US Department of Commerce. https://www.ngdc.noaa.gov/mgg/

Dudhia J (1989) Numerical study of convection observed during the winter monsoon experiment using a mesoscale

two-dimensional model. J Atmos Sci 46(20): 3077–3107. https://doi.org/10.1175/1520-0469(1989)046%3C3077:NSOCOD%3E2.0.CO;2

Dyer AJ, Hicks BB (1970) Flux-gradient relationships in the constant flux layer. Q J R Meteorol Soc 96(410):715–721. https://doi.org/10.1002/qj.49709641012

Emanuel KA (1987) The dependence of hurricane intensity on climate. Nature 326(6112): 483–485. https://doi.org/10.1038/326483a0

Emanuel KA (2003) Tropical cyclones. Annu Rev Earth Planet Sci 31. https://doi.org/10.1146/annurev.earth.31.100901.141259

Emanuel KA (2013) Downscaling CMIP5 climate models shows increased tropical cyclone activity over the 21st century. Proc Natl Acad Sci 110(30):12219–12224. https://doi.org/10.1073/pnas.1301293110

Emanuel KA, Živković-Rothman M (1999) Development and evaluation of a convection scheme for use in climate models. J Atmos Sci 56(11): 1766–1782. https://doi.org/10.1175/1520-0469(1999)056%3C1766:DAEOAC%3E2.0.CO;2

Emanuel K, Solomon S, Folini D, Davis S, Cagnazzo C (2013) Influence of tropical tropopause layer cooling on Atlantic hurricane activity. J Clim 26(7):2288–2301. https://doi.org/10.1175/JCLI-D-12-00242.1

Gualdi S, Scoccimarro E, Navarra A (2008) Changes in tropical cyclone activity due to global warming: results from a high-resolution coupled general circulation model. J Clim 21(20):5204–5228. https://doi.org/10.1175/2008JCLI1921.1

Hill C, DeLuca C, Balaji V, Suarez M, Silva AD (2004) The architecture of the earth system modeling framework. Comput Sci Eng 6(1):18–28. https://doi.org/10.1109/MCISE.2004.1255817

Hong JSG, Lancaster MJ (2004) Microstrip filters for RF/microwave applications, vol 167. Wiley, New York

Jisan MA (2017) An ensemble study of the sea level rise impact on storm surge and inundation in the coastal Bangladesh. Dissertation, Coastal Carolina University

Jisan MA, Bao S, Pietrafesa LJ (2016) Investigating tropical cyclones and its related storm surge & inundation in coastal Bangladesh using a coupled atmosphere-ocean model [A43I-0382] presented at 2016 Fall Meeting, American Geophysical Union, San Francisco, CA, 12–16 Dec

Jisan MA, Bao S, Pietrafesa LJ (2017) Ensemble Projection of the Sea Level Rise Impact on Storm Surge and Inundation in the Coastal Bangladesh. Nat Hazards Earth Syst Sci Discuss. https://doi.org/10.5194/nhess-2017-216 **(in review, 2017)**

Kimura F, Kitoh A (2007) Downscaling by pseudo global warming method. In: Report of research projection on impact of climate changes on agricultural production system in arid areas, Kyoto, pp 43–46

Knutson TR, Tuleya RE, Shen W, Ginis I (2001) Impact of CO_2-induced warming on hurricane intensities as simulated in a hurricane model with ocean coupling. J Clim 14(11):2458–2468. https://doi.org/10.1175/1520-0442(2001)014%3C2458:IOCIWO%3E2.0.CO;2

Knutson TR, Tuleya RE (2004) Impact of CO_2-induced warming on simulated hurricane intensity and precipitation: sensitivity to the choice of climate model and convective parameterization. J Clim 17(18):3477–3495. https://doi.org/10.1175/1520-0442(2004)017%3C3477:IOCWOS%3E2.0.CO;2

Knutson TR, McBride JL, Chan J et al (2010) Tropical cyclones and climate change. Nat Geosci 3(3):157–163. https://doi.org/10.1038/ngeo779

Knutson TR, Sirutis JJ, Vecchi GA et al (2013) Dynamical downscaling projections of twenty-first-century Atlantic hurricane activity: CMIP3 and CMIP5 model-based scenarios. J Clim 26(17): 6591–6617. https://doi.org/10.1175/JCLI-D-12-00539.1

Lin II, Pun IF, Wu CC (2009) Upper-ocean thermal structure and the western North Pacific category 5 typhoons. Part II: Dependence on translation speed. Mon Weather Rev 137(11):3744–3757. https://doi.org/10.1175/2008MWR2277.1

Lin II, Pun IF, Lien CC (2014) "Category-6" supertyphoon Haiyan in global warming hiatus: Contribution from subsurface ocean warming. Geophys Res Lett 41(23):8547–8553. https://doi.org/10.1002/2014GL061281

Lloyd ID, Vecchi GA (2011) Observational evidence for oceanic controls on hurricane intensity. J Clim 24(4):1138–1153. https://doi.org/10.1175/2010JCLI3763.1

Mlawer EJ, Taubman SJ, Brown PD, Iacono MJ, Clough SA (1997) Radiative transfer for inhomogeneous atmospheres: RRTM, a validated correlated-k model for the longwave. J Geophys Res Atmos 102(D14):16663–16682. https://doi.org/10.1029/97JD00237

Noh Y, Cheon WG, Hong SY, Raasch S (2003) Improvement of the K-profile model for the planetary boundary layer based on large eddy simulation data. Bound Layer Meteorol 107(2):401–427. https://doi.org/10.1023/A:1022146015946

Paulson CA (1970) The mathematical representation of wind speed and temperature profiles in the unstable atmospheric surface layer. J Appl Meteorol 9(6): 857–861. https://doi.org/10.1175/1520-0450(1970)009%3C0857:TMROWS%3E2.0.CO;2

Price JF (1981) Upper ocean response to a hurricane. J Phys Oceanogr 11(2): 153–175. https://doi.org/10.1175/1520-0485(1981)011%3C0153:UORTAH%3E2.0.CO;2

Rahaman KM, Ahmed FRS, Islam MN (2016) Modeling on climate induced drought of north-western region, Bangladesh. Model Earth Syst Environ 2(1):45. https://doi.org/10.1007/s40808-016-0089-7

Sakib M, Nihal F, Haque A, Rahman M, Ali M (2015) Sundarban as a buffer against storm surge flooding. World J Eng Technol 3:59–64. https://doi.org/10.4236/wjet.2015.33C009

Sato T, Kimura F, Kitoh A (2007) Projection of global warming onto regional precipitation over Mongolia using a regional climate model. J Hydrol 333(1):144–154. https://doi.org/10.1016/j.jhydrol.2006.07.023

Shay LK, Goni GJ, Black PG (2000) Effects of a warm oceanic feature on Hurricane Opal. Mon Weather Rev 128(5): 1366–1383. https://doi.org/10.1175/1520-0493(2000)128%3C1366:EOAWOF%3E2.0.CO;2

Shen W, Tuleya RE, Ginis I (2000) A sensitivity study of the thermodynamic environment on GFDL model hurricane intensity: implications for global warming. J Clim 13(1):109–121. https://doi.org/10.1175/1520-0442(2000)013%3C0109:ASSOTT%3E2.0.CO;2

Skamarock WC, Klemp JB, Dudhia J, Gill DO, Barker DM, Wang W, Powers JG (2005) A description of the advanced research WRF version 2. NCAR Tech Notes- NCAR/TN-468 + STR

Stewart SR (2017) National Hurricane Center Tropical Cyclone Report: Hurricane Matthew (AL142016). http://www.nhc.noaa.gov/data/tcr/AL142016_Matthew.pdf. Accessed 7 Apr 2017

Stocker T (ed) (2014) Climate change 2013: the physical science basis: Working Group I contribution to the Fifth assessment report of the Intergovernmental Panel on Climate Change. Cambridge University Press, Cambridge

Temam R (1984) Navier-stokes equations, vol 2. North-Holland, Amsterdam, pp xii+-526

Vecchi GA, Fueglistaler S, Held IM, Knutson TR, Zhao M (2013) Impacts of atmospheric temperature trends on tropical cyclone activity. J Clim 26(11):3877–3891. https://doi.org/10.1175/JCLI-D-12-00503.1

Wang S, Camargo SJ, Sobel AH, Polvani LM (2014) Impact of the tropopause temperature on the intensity of tropical cyclones—an idealized study using a mesoscale model. J Atmos Sci 71(11):4333–4348. https://doi.org/10.1175/JAS-D-14-0029.1

Wear DN, Greis JG (2012) The Southern Forest Future Project: summary report. General Technical Report SRS-GTR-168. USDA-Forest Service, Southern Research Station, Asheville

Webb EK (1970) Profile relationships: the log-linear range, and extension to strong stability. Q J R Meteorol Soc 96(407): 67–90. https://doi.org/10.1002/qj.49709640708

Williams JJ, Esteves LS, Rochford LA (2015) Modelling storm responses on a high-energy coastline with XBeach. Model Earth Syst Environ 1(1–2):3. https://doi.org/10.1007/s40808-015-0003-8

Yospin GI, Wood SW, Holz A, Bowman DM, Keane RE, Whitlock C (2015) Modeling vegetation mosaics in sub-alpine Tasmania under various fire regimes. Model Earth Syst Environ 1(3):16. https://doi.org/10.1007/s40808-015-0019-0

Zhao M, Held IM (2010) An analysis of the effect of global warming on the intensity of Atlantic hurricanes using a GCM with statistical refinement. J Clim 23(23):6382–6393. https://doi.org/10.1175/2010JCLI3837.1

Zhao M, Held IM, Lin SJ, Vecchi GA (2009) Simulations of global hurricane climatology, interannual variability, and response to global warming using a 50-km resolution GCM. J Clim 22(24):6653–667. https://doi.org/10.1175/2009JCLI3049.1